Electronic Supplementary Information

# Photo- and Electrochromic Properties of Covalently Connected Symmetrical and Unsymmetrical Spiropyran/Polyoxometalate Dyads

Olivier Oms,[a] Khadija Hakouk,[b] Rémi Dessapt,[b] Philippe Deniard,[b] Stéphane Jobic,[b] Anne Dolbecq,[a] Thomas Palacin,[a] Louis Nadjo,[c] Bineta Keita,[c] Jérôme Marrot[a] and Pierre Mialane[a]

[a] *Institut Lavoisier de Versailles, UMR 8180, Université de Versailles Saint-Quentin, 45 avenue des Etats-Unis, 78035 Versailles Cedex,France. E-mail: mialane@chimie.uvsq.fr*

[b] *Institut des Matériaux Jean Rouxel, Université de Nantes, CNRS, 2 rue de la Houssinière, BP 32229, 44322 Nantes, France. E-mail: remi.dessapt@cnrs-imn.fr*

[c] *Laboratoire de Chimie Physique, UMR CNRS 8000, Equipe d'Electrochimie et Photo électrochimie Université Paris 11, Bâtiment 350, 91405 Orsay Cedex (France.)E-mail: bineta.keita@lcp.u-psud.fr*

## S1 Synthetic procedures

**Chemicals and reagents.** All available chemicals were purchased from major chemical suppliers and used as received: EEDQ (2-ethoxy-1-ethoxycarbonyl-1,2-dihydroquinoline), TRIS (2-Amino-2-(hydroxyméthyl)propane-1,3-diol). The 1-(β-carboxyethyl)-3',3'-dimethyl-6-nitrospiro(indoline-2',2[2H-1]benzopyran) ($SPCO_2H$)[S1.1] photochromic derivative and the Anderson-type polyoxomolybdate $(TBA)_3[MnMo_6O_{18}\{(OCH_2)_3CNH_2\}_2]$[S1.2] have been synthesized as previously described.

NMR spectra were recorded on a Bruker Advance 300 spectrometer operating at 300 MHz for $^1H$. Chemical shifts are expressed in parts per million (ppm) downfield from internal TMS. The following abbreviations are used: s, singlet; d, doublet; t, triplet; m, multiplet; br., broad.

IR spectra: relative intensities are given after the wavenumber as vs = very strong, s = strong, m = medium, w = weak, sh. = shoulder, br. = broad.

Elemental analyses were performed by the Service Central d'Analyse of CNRS, 69390 Vernaison, France.

**Synthesis of SPtris**

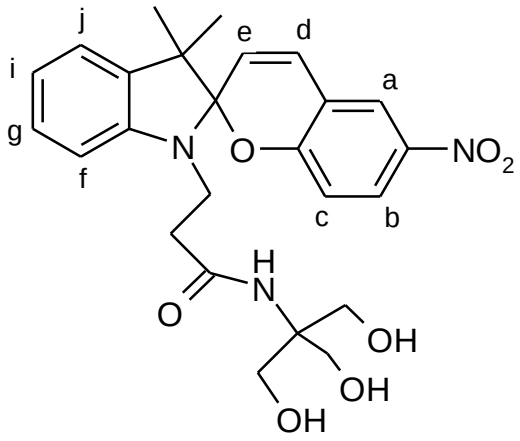


To a suspension of $SPCO_2H$ (500 mg, 1.32 mmol) in EtOH (5 mL) were added EEDQ (390 mg, 1.58 mmol) and TRIS (175 mg, 1.45 mmol) at room temperature. The reaction mixture was stirred overnight at 50°C. The solvent of the resulting purple solution was then removed under vacuum and the residue was dissolved in AcOEt (12 mL). The solution was kept 24 h at

4°C and the resulting precipitate was isolated by filtration, washed with AcOEt (2*3 mL) and $Et_2O$ (2*5 mL). **SPtris** (425 mg, 0.88 mmol) was obtained as a pale pink solid in 67% yield.

$^1$H NMR ($CDCl_3$, 300MHz, 298K) δ 8.03 (m, 2H, Ha and Hb), 7.21 (t, 1H, Hg, J = 7.7 Hz), 7.10 (d, 1H, Hj, J = 7.1 Hz), 6.92 (m, 2H, Hd and Hi), 6.84 (d, 1H, Hc, J = 8.7 Hz), 6.67 (d, 1H, Hf, J = 7.7 Hz), 6.59 (s, 1H, -NH-), 5.86 (d, 1H, He, J = 10.4 Hz), 4.54 (s, br., 3H, -OH), 3.72 (m, 1H, -$CH_2$N-), 3.53 (m, 1H, -$CH_2$N-), 3.48 (s, br., 6H, -$CH_2$O-), 2.60 (m, 1H, -$CH_2$CO-), 2.47 (m, 1H, -$CH_2$CO-), 1.29 (s, 3H, -$CH_3$), 1.16 (s, 3H, -$CH_3$). $^{13}$C NMR ($CDCl_3$, 75MHz, 298K) δ 173.3 (C=O), 159.3, 146.3, 141.1, 135.9, 128.5, 127.8, 126, 122.8, 121.9, 119.9, 118.6, 115.6, 106.7, 62.1, 61.3, 53.0, 39.9, 36.5, 25.8, 19.9. IR (ATR) : ν ($cm^{-1}$) 3314 (m), 2964 (ν C-H, m), 2936 (ν C-H, m), 2872 (ν C-H, m), 1643 (ν C=O, s), 1610 (m), 1578 (m), 1515 (s), 1480 (s), 1459 (s), 1335 (vs), 1268 (vs), 1158 (m), 1126 (m), 1088 (s), 1019 (vs), 949 (vs), 901 (m), 803 (s), 743 (vs), 680 (w), 628 (w), 520 (w). Anal. Calcd for $C_{25}H_{29}N_3O_7$. 0.5 AcOEt (527.6): C, 61.47 ; H, 6.31 ; N, 7.97. Found : C, 61.17 ; H, 6.43 ; N, 8.14.

*Note* : Assignments of protons of spiropyran is based on information given in reference S1.3. We could see by $^1$H NMR that the product contained a small amount of AcOEt that could not be removed under vacuum overnight

**Synthesis of 1, $(TBA)_3[MnMo_6O_{18}\{(OCH_2)_3CNH_2\}\{(OCH_2)_3CNHC_{21}H_{19}N_2O_4\}]$**

To a solution of $(TBA)_3[MnMo_6O_{18}\{(OCH_2)_3CNH_2\}_2]$ (3 g, 1.6 mmol) in $CH_3CN$ (60 mL) were added $SPCO_2H$ (365 mg, 0.96 mmol) and EEDQ (256 mg, 1.04 mmol) at room temperature. The reaction mixture was stirred at 50°C during 18 h. The solvent was removed under vacuum and the residue was dissolved in a minimum of $CH_3CN$. The solution was added to a large quantity of $Et_2O$ (45 mL). The resulting precipitate was then isolated by filtration and placed in acetone (40 mL). The suspension was stirred during 10 minutes and filtered. The solvent of the filtrate was removed under vacuum and the residue was dissolved in a minimum of $CH_3CN$. The solution was added to a large quantity of $Et_2O$. The resulting precipitate was then isolated by filtration. A similar treatment with 12 mL of acetone was effectuated. **1** (503 mg, 0.22 mmol) was finally obtained as a pale pink solid in 23% yield.

$^1$H NMR ($CD_3CN$, 300 MHz, 298K) δ 63.7 (s, br., 12H, -$CH_2$-O), 8.06 (s, 1H), 8.00 (d, 1H, J = 7.9 Hz), 7.20-7.10 (m, 3H), 6.85 (t, 1H, J = 7.1 Hz), 6.71 (m, 2H), 6.46 (br., 1H), 5.89 (d, 1H, He, J = 7.1 Hz), 3.51 (m, 1H), 3.36 (m, 1H), 3.14 (m, 24H, -$NCH_2$- (TBA)), 2.71 (m, 2H),

1.63 (m, 24H, -$NCH_2CH_2$- (TBA)), 1.38 (m, 24H, -$NCH_2CH_2CH_2$- (TBA)), 1.25 (s, 3H, -$CH_3$), 1.13 (s, 3H, -$CH_3$), 0.98 (m, 36H, -$CH_3$ (TBA)).$^{13}$C NMR ($CD_3CN$, 75 MHz, 298K) δ 172.3, 159.4, 146.7, 141.1, 136.1, 128.9, 127.8, 125.6, 123.5, 122.9, 121.7, 119.4, 119.1, 115.4, 107.2, 107, 58.4, 52.6, 40.7, 33.8, 26.1, 23.5, 19.8, 19.1, 13.2. IR (ATR) : ν ($cm^{-1}$) 3285 (w), 2959 (ν C-H, m), 2932 (ν C-H, m ), 2872 (ν C-H, m), 1672 (ν C=O, s), 1610 (m), 1575 (m), 1514 (s), 1480 (s), 1459 (m), 1333 (m), 1273 (m), 1158 (w), 1122 (w), 1087 (m), 1026 (s), 938 (ν Mo=O, vs), 917 (ν Mo=O, vs), 899 (ν Mo=O, vs), 806 (m), 747 (m), 654 (ν Mo-O-Mo, vs, br.), 562 (m). Anal. Calcd for $MnMo_6O_{28}C_{77}H_{142}N_7$ (2244.6): Mn, 2.45 ; Mo, 25.65 ; C, 41.21 ; H, 6.33 ; N, 4.37. Found: Mn, 2.42 ; Mo, 24.92 ; C, 41.19 ; H, 6.41 ; N, 4.33.

**Synthesis of 2, $(TBA)_3[MnMo_6O_{18}\{(OCH_2)_3CNHC_{21}H_{19}N_2O_4\}_2]$**

To a solution of $SPCO_2H$ (462 mg, 1.22 mmol) and EEDQ (324 mg, 1.32 mmol) in $CH_3CN$ (15 mL), $(TBA)_3[MnMo_6O_{18}\{(OCH_2)_3CNH_2\}_2]$ (570 mg, 0.30 mmol) was added at room temperature. The reaction mixture was stirred at 50°C during 48 h. The solvent was removed under vacuum and the residue was dissolved in a minimum of $CH_3CN$. The solution was added to a large quantity of $Et_2O$ (40 mL). The resulting precipitate was then isolated by filtration. This treatment was repeated three times (the last filtrate was no more coloured). **2** (558 mg, 0.21 mmol) was isolated as a pale pink solid in 71% yield.

$^1$H NMR ($CD_3CN$, 300 MHz, 298K) δ 65.02 (s, br., 12H, -$CH_2$-O), 8.06 (s, 2H), 8.00 (d, 2H, J = 8.8 Hz), 7.20-7.10 (m, 6H), 6.85 (t, 2H, J = 7.3 Hz), 6.71 (m, 4H), 6.46 (br., 2H), 5.88 (d, 2H, He, J = 7.7 Hz), 3.52 (m, 2H), 3.35 (m, 2H), 3.12 (m, 24H, -$NCH_2$- (TBA)), 2.71 (m, 4H), 1.62 (m, 24H, -$NCH_2CH_2$- (TBA)), 1.38 (m, 24H, -$NCH_2CH_2CH_2$- (TBA)), 1.24 (s, 6H, -$CH_3$), 1.13 (s, 6H, -$CH_3$), 0.98 (m, 36H, -$CH_3$ (TBA)).$^{13}$C NMR ($CD_3CN$, 75 MHz, 298K) δ 172.3, 159.4, 146.8, 141.1, 136.1, 128.9, 127.8, 125.6, 123.5, 122.9, 121.7, 119.4, 119.1, 115.5, 107.2, 107.1, 58.4, 52.6, 36.7, 26.1, 23.5, 19.7, 19.1, 13.2. IR (ATR) : ν ($cm^{-1}$) 3294 (w), 2960 (ν C-H, m), 2933 (ν C-H, m ), 2871 (ν C-H, m), 1673 (ν C=O, s), 1608 (m), 1575 (m), 1514 (s), 1480 (s), 1459 (m), 1333 (m), 1273 (m), 1159 (w), 1111 (w), 1087 (m), 1063 (m), 1022 (s), 939 (ν Mo=O, vs), 918 (ν Mo=O, vs), 900 (ν Mo=O, vs), 806 (m), 746 (m), 657 (ν Mo-O-Mo, vs, br.), 562 (m). Anal. Calcd for $MnMo_6O_{32}C_{98}H_{160}N_9$ (2607.0) : Mn, 2.11 ; Mo, 22.08 ; C, 45.15 ; H, 6.19 ; N, 4.84. Found : Mn, 2.09 ; Mo, 22.13 ; C, 45.04 ; 6.13 ; N, 4.70.

## S2 Solution $^1$H NMR

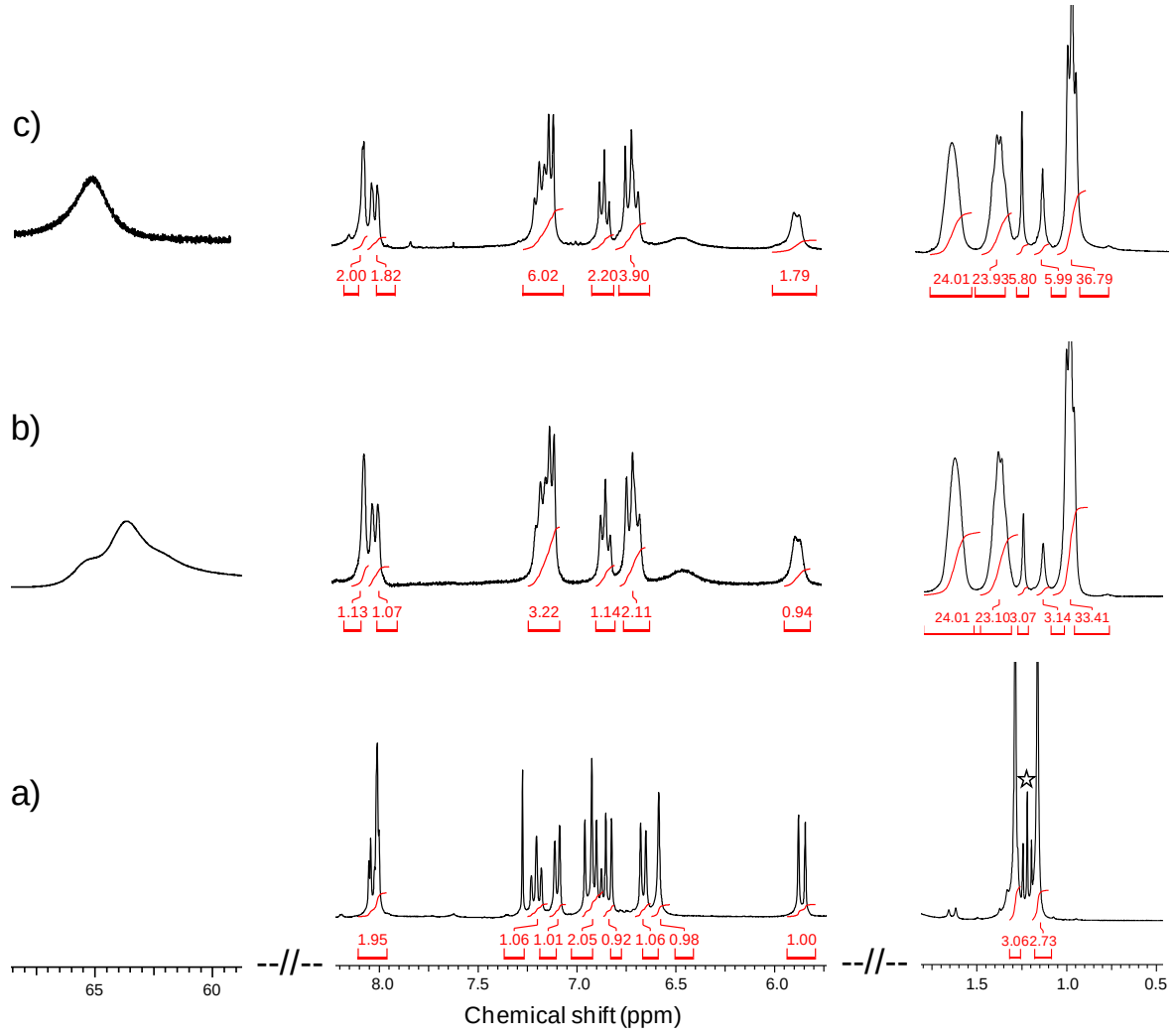


Comparison of the $^1$H NMR spectra for a) **SPtris** (in $CDCl_3$**)** b) **1** (in $CD_3CN$) and c) **2** (in $CD_3CN$) in methyl and TBA region (0.5-1.8 ppm), aromatic region (5.75-8.2 ppm) and in the 59-67 ppm range corresponding to the methylene protons close to the $Mn^{III}$ centre in the organic-inorganic hybrids. Obviously, for **1** and **2**, we observe a different ratio between the integration relative to the TBA protons (signals at 1.62, 1.38 and 0.98 ppm integrated for 24, 24 and 36 protons respectively) and the spiropyran moiety(ies): aromatic region and signals at 1.24 and 1.13 ppm corresponding to the methyl groups (each one is integrated for 3 protons for compound **1**or 6 protons for **2**).

In the spectrum of **SPtris** (a), ☆ indicates the presence of ethyl acetate solvent.

**S3 IR Spectra of 1 and 2**

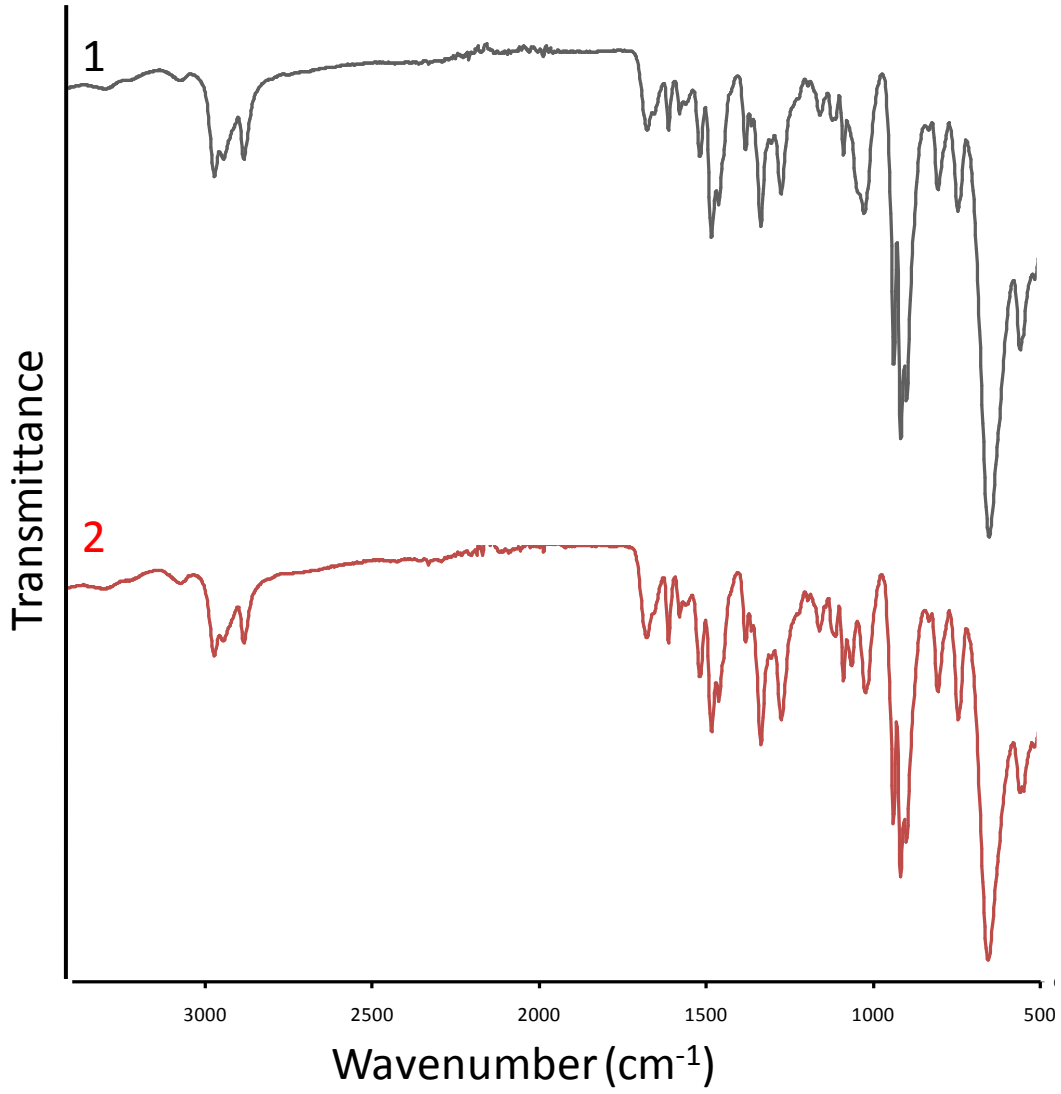

## S4 Single crystal XRD

Intensity data collection on compound **1** was carried out with a Bruker Nonius X8 APEX 2 diffractometer equipped with a CCD bidimensional detector using Mo Kα monochromatized radiation (λ = 0.71073 Å). Due to the very high instability of **1** in the crystalline form at room temperature, the data were recorded at 200K. Moreover, despite numerous efforts, it has also not been possible to avoid a certain loss of crystallinity during the transfer of the crystal from the mother liquor to the diffractometer. The absorption corrections were based on multiple and symmetry-equivalent reflections in the data set using the SADABS program[S4.1] based on the method of Blessing.[S4.2] The structure was solved by direct methods and refined by full-matrix least-squares using the SHELX-TL package.[S4.3] Due to the relatively poor quality of the studied single-crystal ($R[F^2 > 2\sigma(F^2)]$ = 10.09 %), 27 carbon atoms have been refined isotropically. The hydrogen atoms were theoretically located on the basis of the conformation of the supporting atoms. It has not been possible to locate the disordered tetrabutylammonium counter-cations due to severe disorder and the data set was corrected with the program SQUEEZE,[S4.4] a part of the PLATON package of crystallographic software used to calculate the solvent or counter-ions disorder area and to remove its contribution to the overall intensity data.

Crystallographic data for complex **1.**

| | **1** |
|---|---|
| Chemical formula | $C_{77}H_{142}Mn\ Mo_6N_7O_{28}$ |
| $M_r$ *(g.mol$^{-1}$)* | 2244.56 |
| Cell setting, space group | Monoclinic, *P2(1)/c* |
| Temperature (K) | 200 (2) |
| *a*, *b*, *c* (Å) | 23.5641 (18), 32.306 (3), 18.4078 (4) |
| α, β, γ (°) | 90.00, 100.876 (3), 90.00 |
| *V* (Å$^3$) | 13761.5 (17) |
| *Z* | 4 |
| $D_x$ (Mg m$^{-3}$) | 1.083 |
| Radiation type | Mo *K*α |
| μ (mm$^{-1}$) | 0.67 |
| Crystal form, colour | Parallelepiped, colorless |
| Crystal size (mm) | 0.22 × 0.20 × 0.04 |
| Diffractometer | Bruker APEX-II CCD |
| Data collection method | ϕ and ω scans |
| Absorption correction | Multi-scan (based on symmetry-related measurements) |
| $T_{min}$ | 0.8666 |
| $T_{max}$ | 0.9737 |
| No. of measured, independent and observed reflections | 116528, 19085, 8669 |
| Criterion for observed reflections | $I > 2\sigma(I)$ |
| $R_{int}$ | 0.0746 |
| $\theta_{max}$ (°) | 23.09 |
| Refinement on | $F^2$ |
| $R[F^2 > 2\sigma(F^2)]$, $wR(F^2)$, *S* | 0.1009, 0.2926, 1.019 |
| No. of relections | 8669 reflections |
| No. of parameters | 456 |
| H-atom treatment | Constrained to parent site |
| Weighting scheme | Calculated $w = 1/[\sigma^2(F_o^2) + (0.1773P)^2 + 0.0000P]$ where $P = (F_o^2 + 2F_c^2)/3$ |
| $(\Delta/\sigma)_{max}$ | 0.121 |
| $\Delta\rho_{max}$, $\Delta\rho_{min}$ (e Å$^{-3}$) | 1.516, –0.87 |

**S5.**

Diffuse reflectivity was measured from 250 to 1000 nm with a 2 nm step using Halon powder (from Varian) as reference (100% reflectance). The reflectivity data were treated by a Kubelka-Munk transformation[S5.1] to obtain the corresponding absorption data and hence better locate the absorption thresholds. The samples were irradiated with a Fisher Bioblock labosi UV lamp ($\lambda_{exc}$ = 365 nm, P = 12W).

Kubelka-Munk transformed reflectivity *vs* wavelength and energy of **1** (—), **2** (—), **SPtris** (—), and $(TBA)_3[MnMo_6O_{18}\{(OCH_2)_3CNH_2\}_2]$ (—). The weak absorption in the visible in the spectra of **1**, **2** and **SPtris** is assignable to a small amount of the merocyanine form which is responsible for the pinkish-white color of the powdered samples.

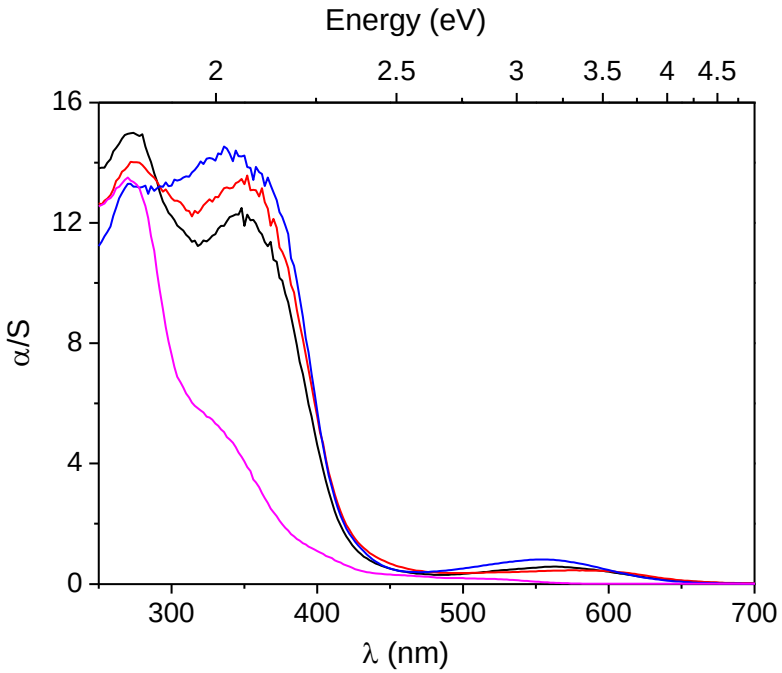

**S6.** Top: Evolution of the color of **2** powder at different 365 nm-UV irradiation time. Bottom: Kubelka-Munk transformed reflectivity of **2** after 0, 0.333, 0.666, 1, 1.5, 2, 3, 4, 6, 10, 15, and 30 min of irradiation at 365 nm.

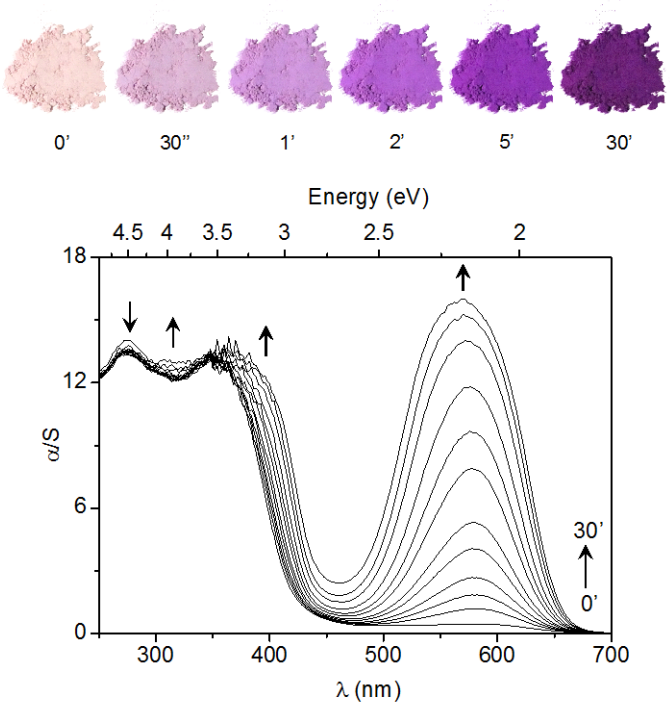

**S7.** Kubelka-Munk transformed reflectivity of **SPtris** after 0, 0.333, 0.666, 1, 1.5, 2, 3, 4, 6, 10, 15, and 30 min of irradiation at 365 nm. Color of **SPtris** microcrystallized powder after 30 min of irradiation at 365 nm.

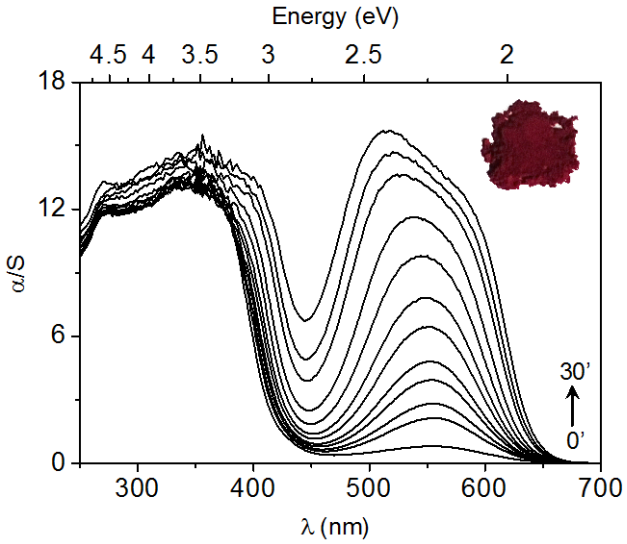

**S8.** Evolution of the photo-generated absorption Abs(t) versus the irradiation time *t* of (a) **1**, (b) **2** and (c) **SPtris** under UV excitation at 365 nm. Abs(*t*) is defined as Abs(*t*) = –ln (R(*t*)/R(0)), with R(*t*) the reflectivity at the time *t* and R(0) the reflectivity at t = 0, i.e. just before UV irradiation.

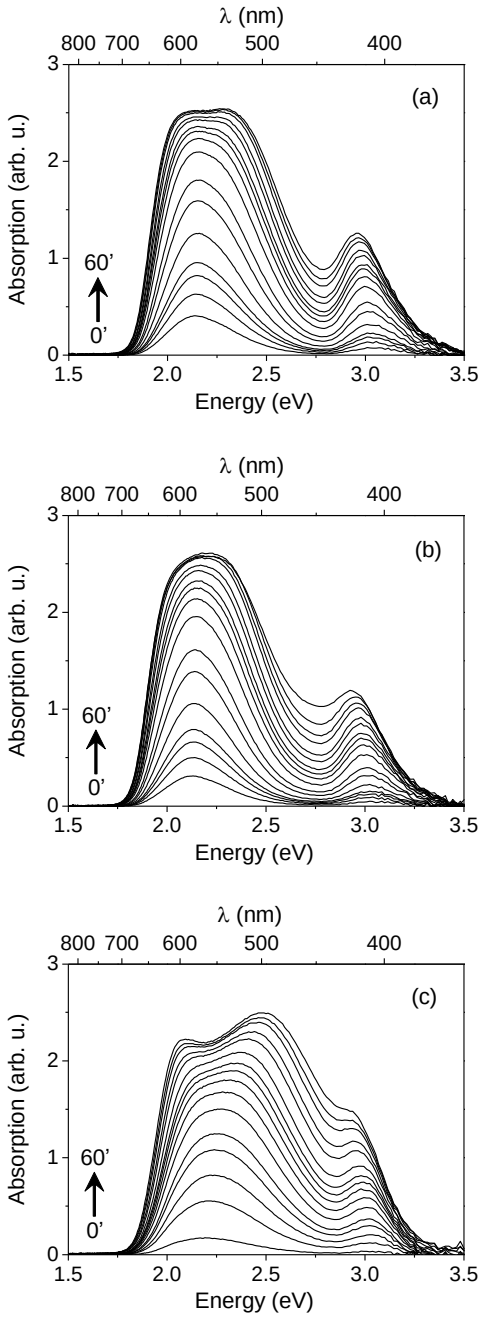

**S9.** Optical characteristics and coloration kinetic parameters of **1**, **2**, and **SPtris**.

| | **1** | **2** | **SPtris** |
|---|---|---|---|
| $A_0$ | 2.290 | 2.189 | 2.493 |
| $A_1$ | -1.133 | -1.087 | -1.238 |
| $k_1$ ($min^{-1}$) | 0.651 | 0.489 | 0.412 |
| $k_2$ ($min^{-1}$) | 0.143 | 0.108 | 0.055 |
| $R^2$ | 0.9996 | 0.9998 | 0.9994 |

The Abs(*t*) *vs t* curves have been fitted as $Abs(t) = A_0 + A_1(\exp(-k_1 t) + \exp(-k_2 t))$ with $k_1$ and $k_2$ the coloration rate constants. $R^2$ is the regression coefficient for the Abs(*t*) *vs t* plots.

# S10. Electrochemistry and Spectroelectrochemistry data

## Electrochemistry materials, apparatus and procedures

For electrochemical experiments, the source, mounting and polishing of the glassy carbon (GC, Le Carbone Lorraine, France) electrodes has been described previously.[S10.1] The electrochemical set-up was an EG & G 273 A driven by a PC with the M270 software. Potentials are measured against a saturated calomel reference electrode (SCE). The counter electrode was a platinum gauze of large surface area. Freshly distilled DMF was used throughout. The solutions were deaerated thoroughly for at least 30 minutes with pure argon and kept under a positive pressure of this gas during the experiments. The supporting electrolyte was 0.2 M $LiClO_4$ in DMF. Spectroelectrochemical experiments were performed in a three-compartment cell comprising a 1-cm optical path quartz cuvette. The working electrode was a sheet of GC (V25, Le Carbone Lorraine, France). The whole cell remained inserted in the spectrophometer cavity and kept under continuous argon bubbling and stirring during electrolyses. A second 1-cm quartz cell was matched with that of the electrochemical cell and served as a reference. UV-Visible spectra were recorded on a Perkin-Elmer Lambda 750 spectrophotometer. Experiments were performed at the laboratory temperature. A photograph of a quartz cuvette featuring the color observed before electrolysis is displayed in Figure S10.1 (electrodes not shown). The bulk colours cut from such cuvettes during the electrolysis are shown in the main text.

Figure S10.1A: spectroelectrochemical cell containing $2.36 \times 10^{-4}$ M **1** (electrodes not shown).

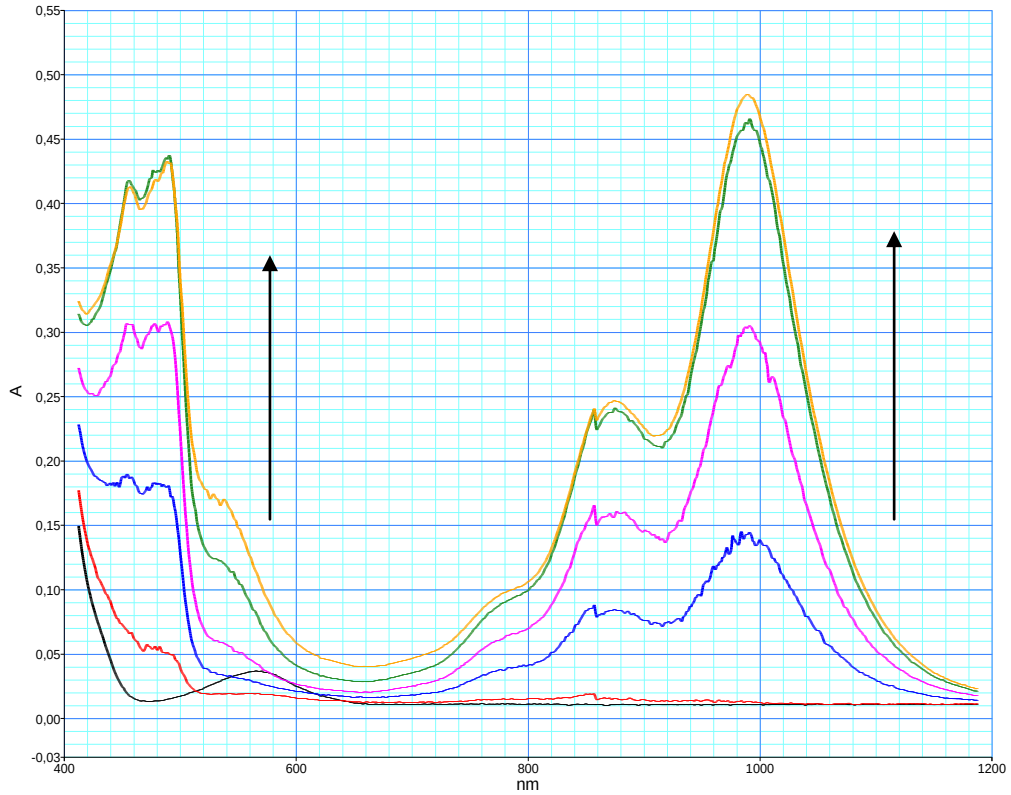


Figure S10.1B: Spectral evolution of **SPtris** during its electro-oxidation.

**Electrochemical characterization of the various species**

*Note*: SPtris refers to the spiropyran entity(-ies) present in **1** and **2** whereas **SPtris** denotes the pure organic ligand. **$MnMo_6(tris)_2$** refers to the polyoxomolybdate cluster $(TBA)_3[MnMo_6O_{18}\{(OCH_2)_3CNH_2\}_2]$[S1.2].

The electroactive centers of these molecules are both oxidisable (Mn and SPtris centers) or reducible (Mn, SPtris and Mo centers). On the corresponding cyclic voltammograms, their peak potentials are observed successively in that order when the potential is scanned respectively in the positive direction for oxidation processes and in the negative direction for reduction processes. It happens that these two groups of processes are well-separated in potential and will therefore be sequentially studied for clarity.

On the oxidation side, the $Mn^{IV}/Mn^{III}$ process is featured by a well-behaved cyclic voltammogram. The results are illustrated for complex **1** selected as a representative. Figure S10.2a shows this wave as a function of the potential scan rate. An excellent linearity is observed for the peak current with the square root of the scan rate, thus indicating a diffusion controlled behavior (Figure S10.2b). The oxidation peak potential is located at $E_p$ = +0.774 V vs SCE with the anodic to cathodic peak potential difference $\Delta E_p$ = 80 mV at v = 0.1V $s^{-1}$. Controlled potential coulometry at E = +0.850 V vs SCE gives a value of 1.04 electron per molecule, in agreement with expectations. Figure S10.3a shows the voltammetric pattern observed when the potential is scanned more positively to reveal the SPtris oxidation wave. The potential location of the broad overlapping reduction wave accompanying the SPtris oxidation upon potential reversal should not be interpreted as a chemical reversibility, but is rather indicative of formation of a new species.[S11.2] In agreement with this interpretation, Figure S10.3b confirms that during the second scan of the CV up to SPtris oxidation, a new broad oxidation pattern was observed which can undergo reversible electrochemistry.[S10.2, S10.3] However, the drop in the SPtris peak intensity indicates the apparent absence of any electrochemical pathway back to SPtris from the oxidation species of the molecule **1**. Finally, we also compared the potential locations for **1**, **2** and **$MnMo_6(tris)_2$**. SPtris substituents appear to shift the oxidation potential in the positive direction based on their number. From **$MnMo_6(tris)_2$** to **2**, the following values were measured $\Delta E_{\mathbf{1}\rightarrow \mathbf{MnMo6(tris)2}}$ = 25 mV and $\Delta E_{\mathbf{2}\rightarrow \mathbf{MnMo6(tris)2}}$ = 50 mV. At the very least, this observation would feature an electron withdrawing ability of the SPtris substituent from the $Mn^{III}$ center.

On the reduction side, Figure S10.4 shows the superposition of the voltammetric patterns of **$MnMo_6(tris)_2$** and **1**. Considering **$MnMo_6(tris)_2$** and scanning the potential in the negative direction, the reduction of $Mn^{III}$ to $Mn^{II}$ is observed first (Ep = - 1 V vs SCE), followed by that of Mo centers (Ep = -1.745 V vs SCE). On potential reversal, the $Mn^{III}/Mn^{II}$ process assumes a quasi reversible behavior and the re-oxidation of Mo centers is represented by two broad oxidation waves. The chemical reversibility of the voltammetric pattern of Mo centers should be noted because a contradictory claim is found in the literature: as a matter of fact, the reduction of $d^0$ Mo centers to the $d^1$ state within Anderson-type anions is expected to be irreversible.[S10.4] However, the present observation was repeatedly confirmed (*vide infra*). It is worth noting that the CV of **$MnMo_6(tris)_2$** was not published previously. Consequently,

further work is planned to understand this behavior. As expected, a multielectron process is observed for the Mo center.[S10.4] In the case of **1**, the voltammetric pattern displays an additional broad wave featuring the reduction the SPtris center and located between the Mn and Mo reduction centers. Actually, the potential locations of the Mn and Mo centers within **1** are slightly more positive than in **$MnMo_6(tris)_2$**. This observation is in agreement with the parallel behavior described for the oxidation process of the Mn center in **1**. Controlled potential coulometry at E = -1.1 V vs SCE gives a value of 1.02 electron per molecule for $Mn^{III} \rightarrow Mn^{II}$ reduction within **1** and 1.08 electron per molecule in **$MnMo_6(tris)_2$** . During these electrolyses, a very pale yellow color was observed for $Mn^{II}$. As concerns Mo centers within **1**, a decrease in their reversibility is noted. Furthermore, comparison of the oxidation waves of **$MnMo_6(tris)_2$** and **1** suggests that the presence of the Anderson POM imparts some stability to **1** relative to **$MnMo_6(tris)_2$** (*vide infra*). Finally, it is worth noting by comparison of the patterns of **$MnMo_6(tris)_2$** and **1**, that the Mo wave within **1** is partly engulfed in the SPtris wave, a behavior tentatively attributable to the very large peak of SPtris (*vide infra*). Figure S10.5 compares the voltammetric patterns of **1** and **2**. The salient feature is that the current intensity of the SPtris center within **2** is twice as large as the corresponding wave of **1**, as expected. This behavior of **2** renders the Mn wave less separated from the SPtris wave.

Finally, we set out to check whether mere stepwise addition up to the appropriate stoichiometry of the POM and **SPtris** would simulate **1** and show the same voltammetric pattern. Figure S10.6a sketches the main patterns of interest. It is worth noting that the two species should display different diffusion coefficients. Starting with the POM, the striking observation following gradual addition of **SPtris** is that the Mo wave is well-separated from the **SPtris** wave and well-behaved. Then, the mixing up of the two waves begins. Ultimately, when the stoichiometry is reached, partial engulfment of the Mo wave is obtained. Strikingly, this Mo wave is irreversible, clearly at variance with the voltammetric behavior of **1**. Figure S10.6b shows in superposition the cyclic voltammograms of **1** and simulated **1**. Our observations would indicate that covalently bonding the SPtris and the POM to create **1** generates voltammetric behaviors not present in the mixture of the components.

**Spectroelectrochemical characterization of SPtris,1 and 2 in the reductive domain**

Detailed evolution of spectra during reduction processes is represented on Figures S10.7, S10.8 for **SPtris**, S10.9 and S10.10 respectively for **1** and **2**. All these spectra display a peak at 420 nm followed by a shoulder around 550 nm associated with the color of reduced MC. This shoulder is hardly visible on the spectrum of **SPtris** during the electrolysis of the latter. However, as soon as the system is switched to open circuit, this band appears and its intensity increases at the expense of the peak at 420 nm, up to a saturation point from which its gradual decrease was observed in favor of the peak at 420 nm (Figure S10.8). Consequently, for **SPtris**, in contrast with **1** and **2**, the electrolysis must be stopped before observing the color of reduced MC. Figure S10.11 compares the spectra of the reduced forms of **SPtris**, **1** and **2** during the electrolysis. It must be noted that the shoulder around 550 nm in **1** is shifted to the red related to that in **2**.

**Remarks on electrochromism**

The favorable redox properties of the **$MnMo_6(tris)_2$**/spiropyran hybrids induce distinct electrochromic states in the same molecule. In particular, the different redox states of the Mn center generate a set of colors associated or not to those of the SP centers. The nuances of colors described in this work were obtained during partial electrolyses (ca 60 % relative to Mn). Thus pure yellow ($Mn^{II}$), or brown ($Mn^{IV}$) and their mixtures with respectively reduced MC and oxidised MC colors were obtained. The reduction of Mo centres deepens the red color of the $Mn^{II}$ and reduced MC mixture. Due to the observed redox potentials of Mn and SP, the Mn center is able to capture electrons from the reduced SP (or vice versa for oxidation process) thus providing a straightforward pathway for the fading processes. It is worth noting that the fading process of the mixture of colors observed after reduction of Mo centres is very slow.

Both for electro-oxidation and electro-reduction, more detailed investigations of the mechanistic pathways of formation of the species which induce the color sets remain a future challenge. For example, the influence of key parameters such as solution temperature will be studied.

.

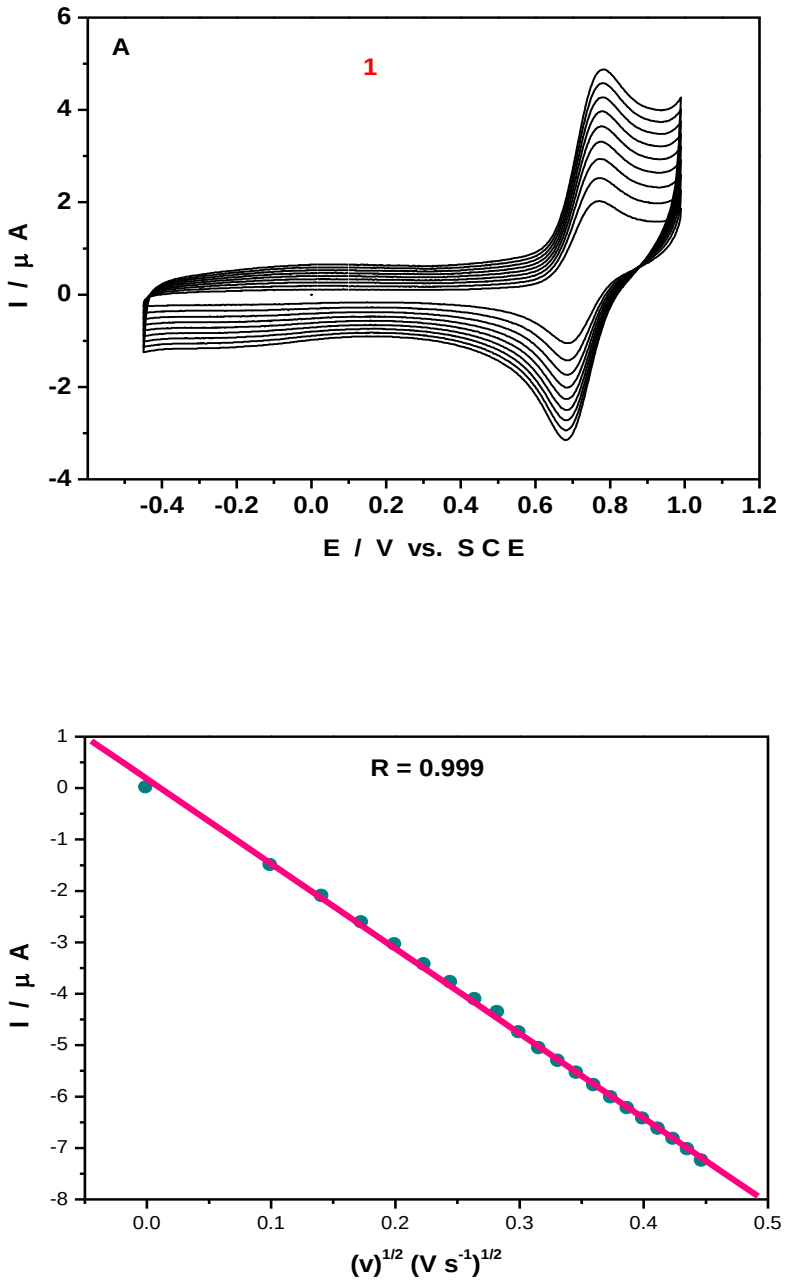


Figure S10.2: Cyclic voltammograms (CVs) and peak current intensity variations of $2.36 \times 10^{-4}$ M **1**. (A) Cyclic voltammograms (CV) of $Mn^{IV}/Mn^{III}$ center within **1** as a function of scan rate (from 10 to 100 mV $s^{-1}$)**;** (B) variation of the anodic peak current intensity as a function the square root of the scan rate. The electrolyte was DMF + 0.2M $LiClO_4$.The reference electrode was a saturated calomel electrode (SCE).

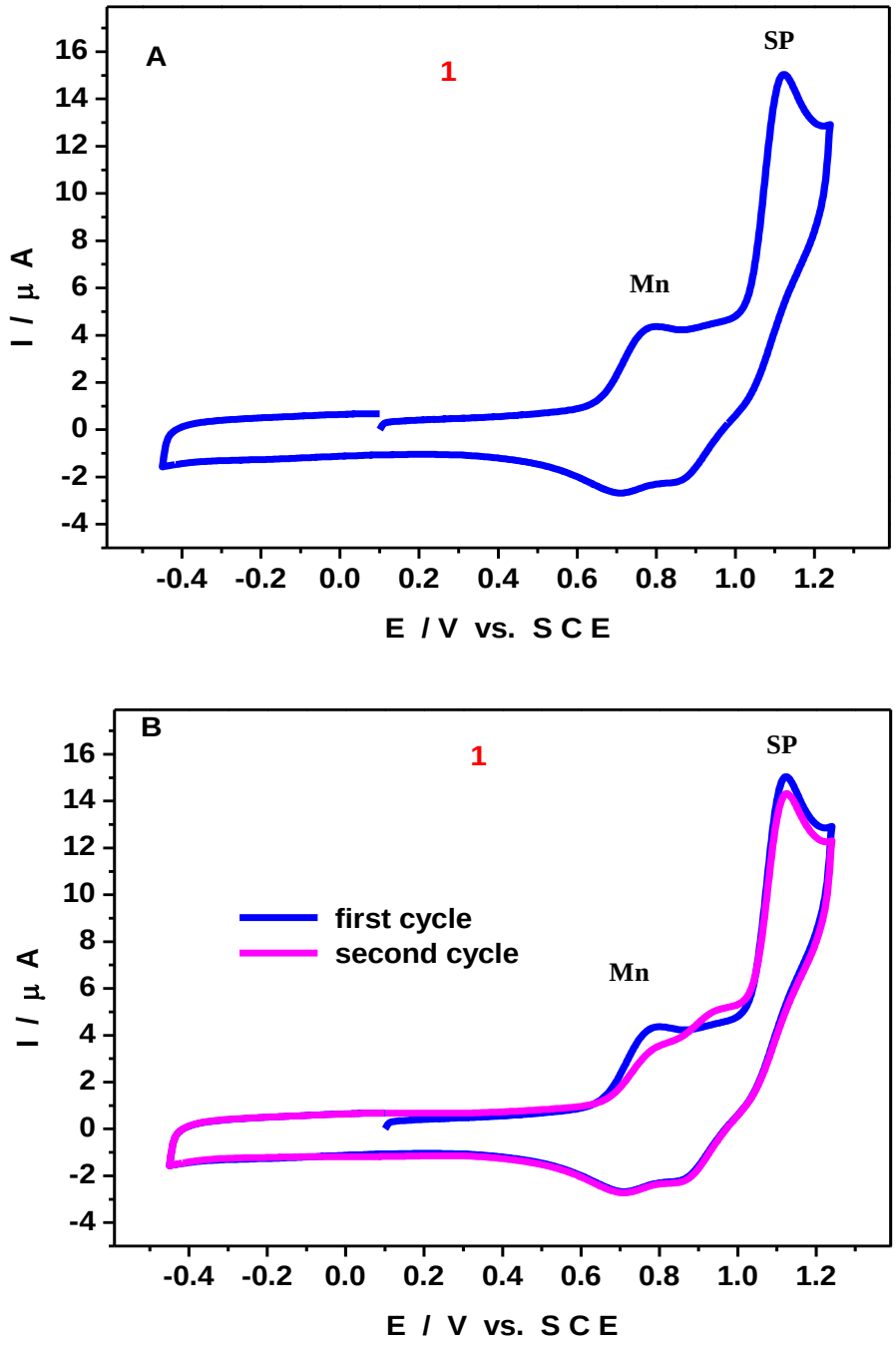


Figure S10.3: Oxidation cyclic voltammograms (CVs) of $2.36 \times 10^{-4}$ M **1** (Mn and SP centers). (A) first cycle**;** (B) first two cycles. The electrolyte was DMF + 0.2M $LiClO_4$.The reference electrode was a saturated calomel electrode (SCE). The scan rate was 0.1V $s^{-1}$.

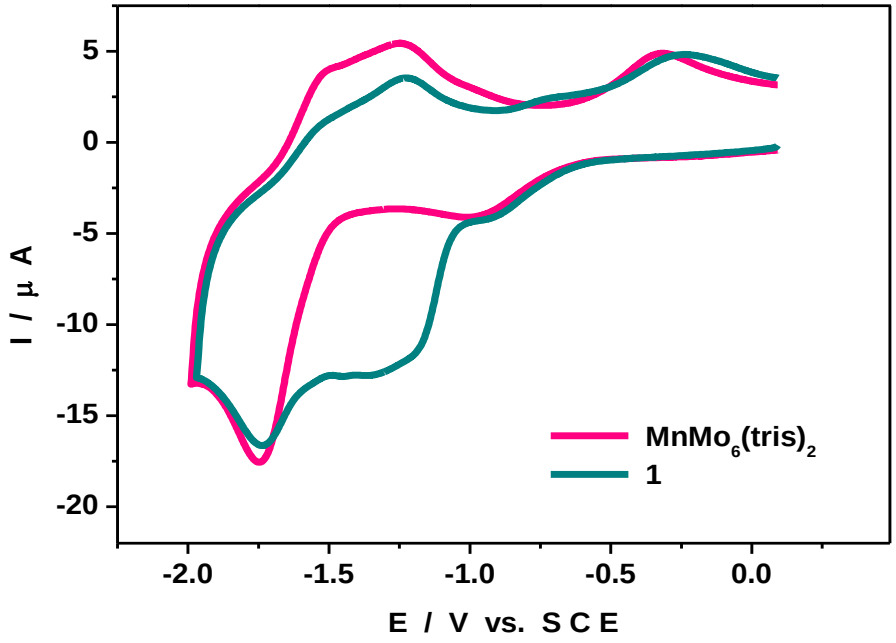


Figure S10.4: Reduction cyclic voltammograms (CVs) of $2.36 \times 10^{-4}$ M **1** (Mn, SP and Mo centers). The electrolyte was DMF + 0.2M $LiClO_4$. The reference electrode was a saturated calomel electrode (SCE). The scan rate was 0.1V $s^{-1}$.

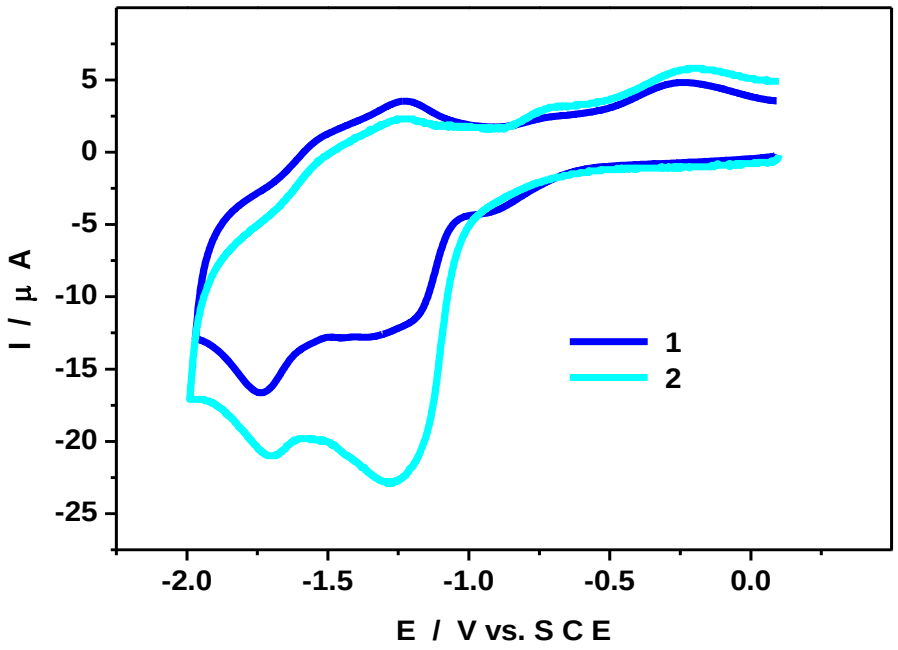


Figure S10.5: Superimposition of reduction cyclic voltammograms (CVs) of **1** and **2** ($2.36 \times 10^{-4}$ M) (Mn, SP and Mo centers). The electrolyte was DMF + 0.2M $LiClO_4$. The reference electrode was a saturated calomel electrode (SCE). The scan rate was 0.1V $s^{-1}$.

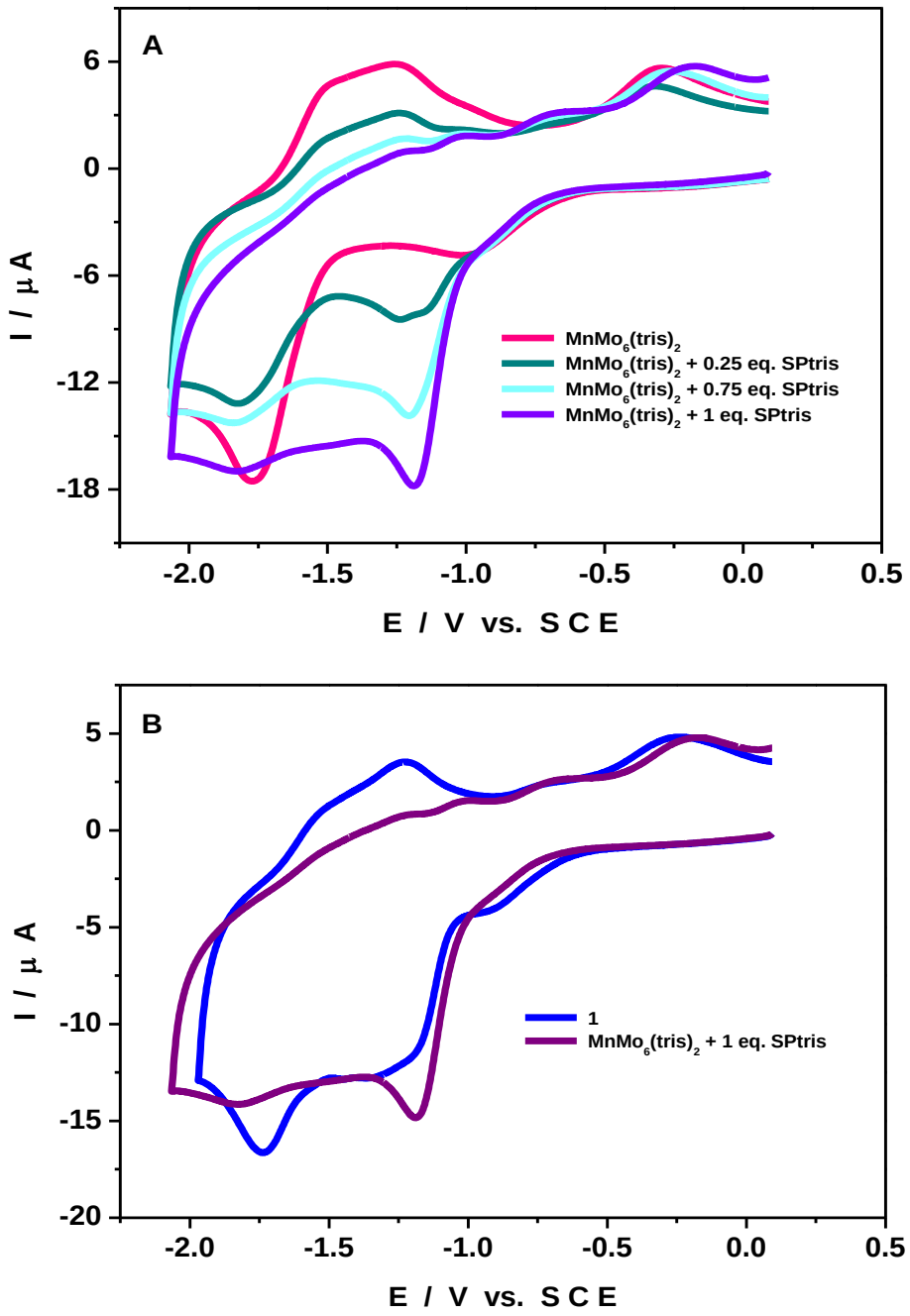


Figure S10.6: Reduction cyclic voltammograms (CVs) of **1** and mixtures of **$MnMo_6(tris)_2$** and **SPtris**; (A) Evolution of the CVs as a function of gradual addition of **SPtris**; (B) Comparison of CVs of **1** and that of the stoichiometric mixture (**$MnMo_6(tris)_2$** + 1 eq. **SPtris**). The electrolyte was DMF + 0.2M $LiClO_4$. The reference electrode was a saturated calomel electrode (SCE). The scan rate was 0.1V $s^{-1}$.

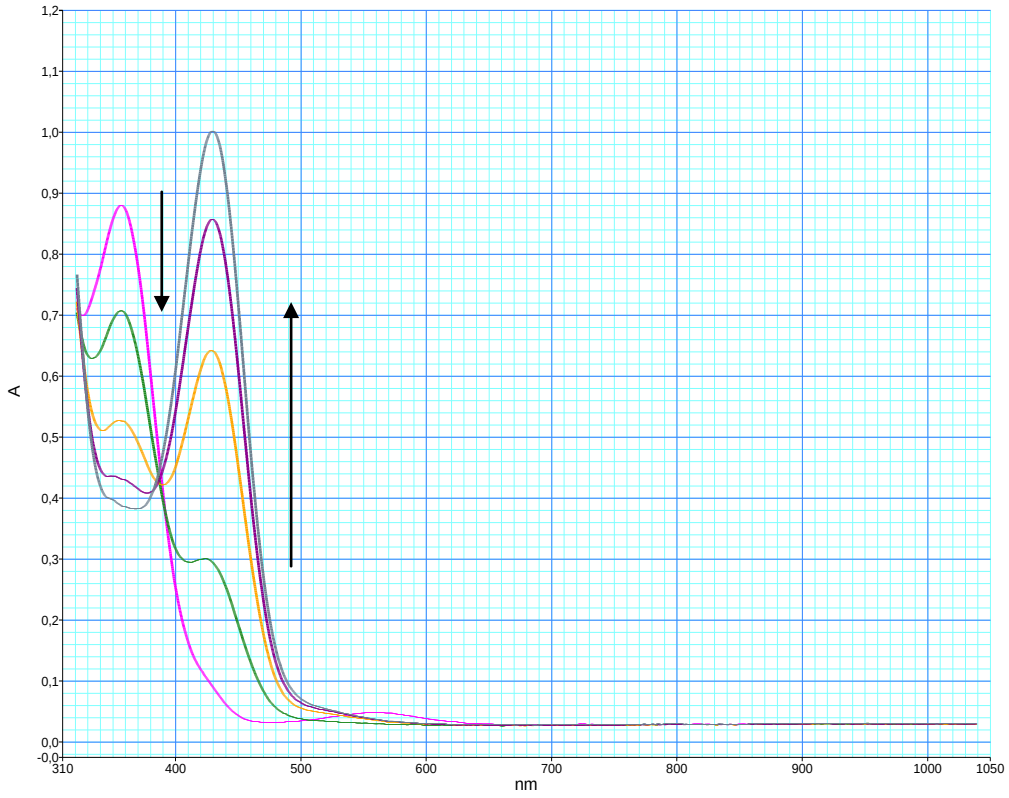


Figure S10.7: Spectral evolution of **SPtris** during its electroreduction.

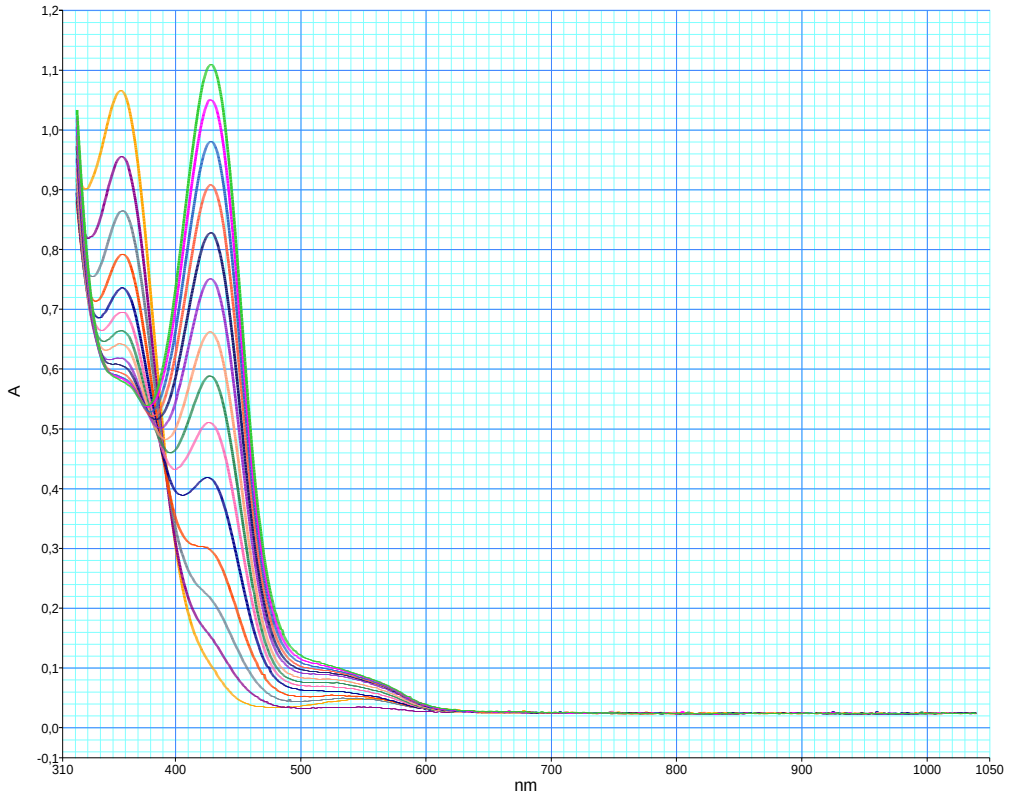


Figure S10.8: Spectral evolution of **1** during its electroreduction.

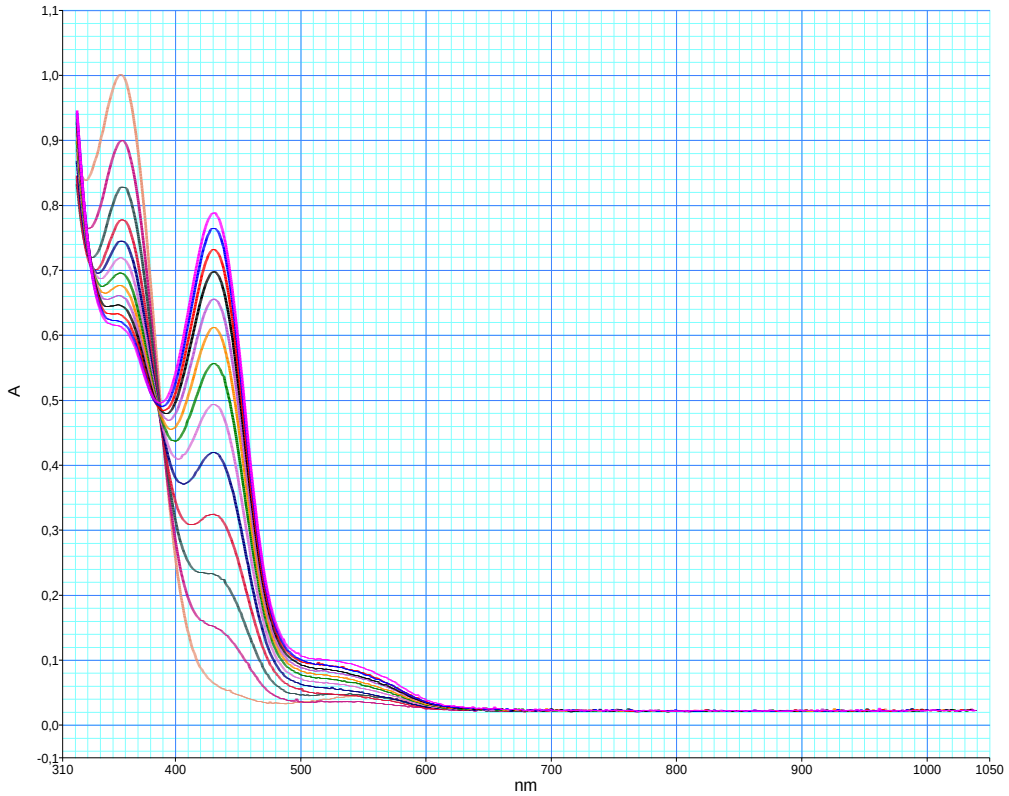


Figure S10.9: Spectral evolution of **2** during its electroreduction

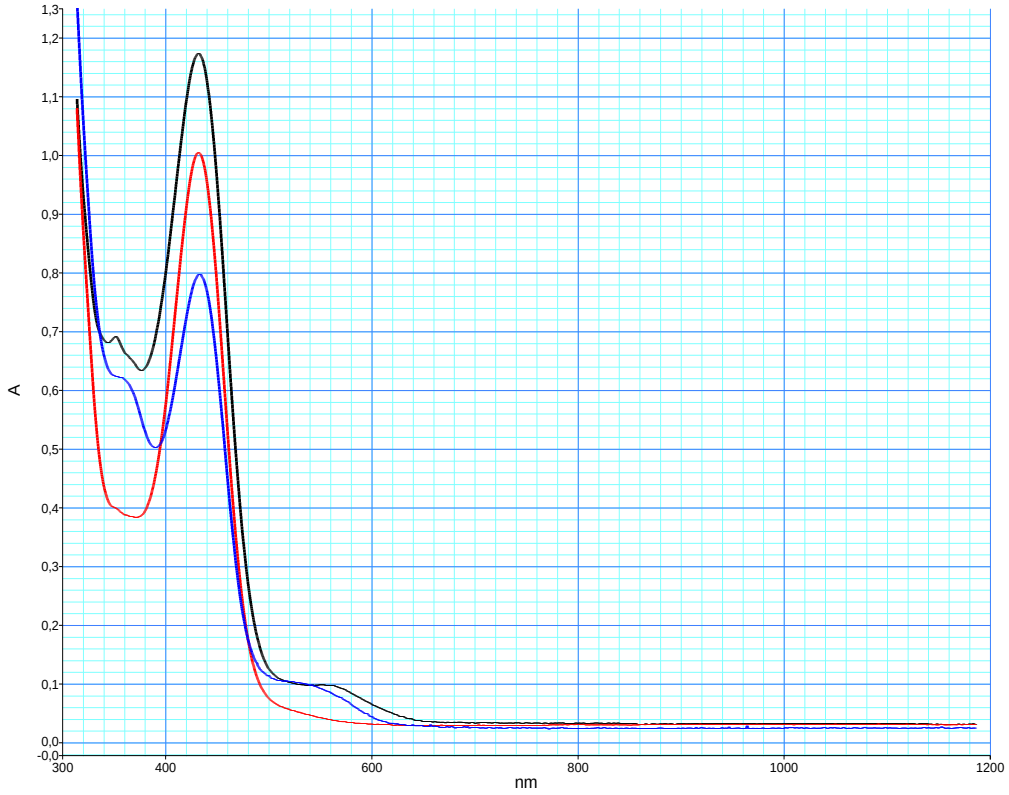


Figure S10.10: Spectra of electro-reduced species of **SPtris** (red), **1** (black) and **2** (blue).

## S11 References


S1.1 A. Fissi, O. Pieroni, G. Ruggeri and F. Ciardelli, *Macromolecules*, 1995, **28**, 302.

S1.2 P.R. Marcoux, B. Hasenknopf, J. Vaissermann and P. Gouzerh, *Eur. J. Inorg. Chem*., 2003, 2406.

S1.3 A. Nayak, H. Liu and G. Belfort, *Angew. Chem. Int. Ed*., 2006, **45**, 4094.

S4.1 G. M. Sheldrick, SADABS, program for scaling and correction of area detector data, University of Göttingen, Germany, 1997.

S4.2 R. Blessing, *Acta Crystallogr.* 1995, **A51**, 33.

S4.3 G. M. Sheldrick, SHELX-TL version 5.03, Software Package for the Crystal Structure Determination, Siemens Analytical X-ray Instrument Division, Madison, WI USA, 1994.

S4.4 P. van der Sluis and A. L. Spek, *Acta Crystallogr., Sect. A.*, 1990, **46**, 194.

S5.1 P. Kubelka and F. Munk, *Z. Techn. Physik* 1931, **12**, 593-601.

S10.1 B. Keita and L. Nadjo *J. Electroanal. Chem.* 1988, **243**, 87-103.

S10.2 K. Wagner, R. Byrne, M. Zanoni, S. Gambhir, L. Dennany, R. Breukers, M. Higgins, P. Wagner, D. Diamond, G. G. Wallace and D. L. Officer, *J. Am. Chem. Soc.*, 2011, **133**, 5453.

S10.3 R. T. F. Jukes, B. Bozic, F. Hartl, P. Belser and L. De Cola, *Inorg. Chem.* 2006, **45**, 8326.

S10.4 M. T. Pope *Heteropoly and Isopoly Oxometalates*, Springer-Verlag, Berlin, 1983**.**